Silicon on a graphene nanosheet with triangle- and dot-shape: Electronic structure, specific heat, and thermal conductivity from first-principle calculations

Hunar Omar Rashid[a], Nzar Rauf Abdullah[a,b,c,*], Vidar Gudmundsson[c]

[a] Division of Computational Nanoscience, Physics Department, College of Science, University of Sulaimani, Sulaimani 46001, Kurdistan Region, Iraq
[b] Komar Research Center, Komar University of Science and Technology, Sulaimani 46001, Kurdistan Region, Iraq
[c] Science Institute, University of Iceland, Dunhaga 3, IS-107 Reykjavik, Iceland

ARTICLE INFO

ABSTRACT

The electronic structure, specific heat, and thermal conductivity of silicon embedded in a monolayer graphene nanosheet are studied using Density Functional Theory. Two different shapes of the substitutional Si doping in the graphene are studied, a triangular and a dot shape. The silicon doping of a graphene nanosheet, with the silicon atoms arranged in a triangular configuration in ortho- and para-positions, opens up a band gap transforming the sheet to a semiconducting material. The opening of the band gap is caused by the presence of the repulsion force between the silicon and carbon atoms decreasing the density of states around the Fermi energy. Consequently, the specific heat and the thermal conductivity of the system are suppressed. For graphene nanosheet doped with a dot-like configuration of silicon atoms, at the ortho-, meta-, and para-positions, the valence band crosses the Fermi level. This doping configuration increases the density of state at the Fermi level, but mobile charge are delocalized and diminished around the silicon atoms. As a result, the specific heat and the thermal conductivity are enhanced. Silicon substitutionally doped graphene nanosheets may be beneficial for photovoltaics and can further improve solar cell devices by controlling the geometrical configuration of the underlying atomic systems.

Introduction

A graphene nanosheet is a 2D material with remarkable qualities in terms of mechanical [1], electrical [2], chemical [3], optical [4], and thermal [5] properties. The investigation of a single layer graphene and its characteristics [6] has paved the way to generate enormous interest and intense activity in graphene research [7,8]. The graphene material has been used as the basic building block for graphitic materials with different directions. It may be wrapped up into zero-dimensional fullerene [9,10] leading to the improvement of the band gap [11], rolled into one-dimensional nanotubes [12], or stacked into three-dimensional graphite [13]. According to the atomic arrangement, the graphene structures can be classified into two categories which are "zigzag" and "armchair". These two types of graphene have different electronic characteristics, especially the creation of non-bonding edge states localized in the zigzag-shaped edges and electron wave interference in the armchair-shaped ones play important roles in the functionality of graphene [14]. The two types, "zigzag" and "armchair", can be constructed in the form of graphene nanoribbons which are promising structures in electron transport [15–17].

The physical properties of graphene can be controlled by doping, which is the process of adding impurities to intrinsic graphene. For instance, silicon, Si, doped graphene has emerged as new 2D materials called siligraphenes, demonstrating attractive optical properties and extreme thermal stability [18,19]. The band gap of siligraphenes depends on the ratio of the Si doping, that is determined by the relationship between the reactants and products in a chemical reaction producing the graphene [20,21]. One can expect to use g-SiC$_2$ for solar cell materials due to the opening band gap, 1.09 eV [20]. Increasing the ratio of Si doping to construct g-SiC$_3$ and g-SiC$_5$, the characteristics of a topological insulator appear in g-SiC$_3$ [22] and g-SiC$_5$ emerges as a semi-metal with excellent gas sensing properties [23]. Furthermore, in g-SiC$_7$ the band gap is increased to 1.13 eV actively encouraging photovoltaics devices within the visible light range [19].

Recently, there has been an increased and strong motivation to explore thermal characteristics of graphene and related composite

* Corresponding author.
  E-mail addresses: nzar.r.abdullah@gmail.com, nzar.abdullah@univsul.edu.iq (N.R. Abdullah).

materials from the technological point of view. Electrical and thermal measurements of siligraphenes have shown that g-SiC can be seen as fascinating material with interesting properties [24]. It has been demonstrated that the thermal properties of g-SiC$_3$ are better compared to g-SiC$_7$, and the thermal conductivity of g-SiC$_7$ is exponentially enhanced with temperature but for g-SiC$_3$ it is parabolically changed [25]. Exploration has shown that the effective thermal conductivity in an optimized mixture of graphene and multilayer graphene can be enhanced [5]. Furthermore, both graphene and graphite at room temperature can be utilized to increase the efficiency of solar cell devices due to a high-recorded thermal property dominated by the acoustic phonons [26].

Motivated by the aforementioned studies, we model a graphene and siligraphene nanosheets. The electronic and the thermal characteristics are studied using Density Functional Theory (DFT). We model two different shapes of substitution Si doping in the graphene: triangle and "dot" shapes. In the triangle shape the Si-atoms are substitutionally embedded in the ortho- and para-positions of the honeycomb structure of graphene. This opens up a band gap leading to the suppression of thermal conductivity. In the "dot" shape, the Si-atoms are substitutionally doped in the ortho-, para-, and meta-positions of graphene. In the "dot" structure, the enhancement of thermal properties of the system is observed.

In Section "Model" the structure of graphene nanosheet is briefly overviewed. In Section "Results" the main achieved results are analyzed. In Section "Conclusion" the conclusion of the results is presented.

Model

We model a monolayer graphene nanosheet consisting of a 3×3 supercell with a diamond shape that is comprised from 32 carbon atoms. We consider the vacuum space in z-axis to be 9.74 Å. The convergence of the SCF calculation is set to 10^{-3} eV, and the geometry of the system is fully relaxed with a Gamma-centered $8 \times 8 \times 1$ k-mesh for both pure and doped graphene nanosheets until the calculated force is smaller than 0.008 eV/Å. In addition to the pristine graphene, we consider two geometrical shapes of Si-atoms in doped graphene, the triangle and the "dot" shape. The triangle Si doped graphene is formed if two Si-atoms are put at the ortho-positions (green) and one Si-atom is placed in a para-position (red) as is shown in Fig. 1. The "dot" Si doped graphene can be built by adding two Si-atoms at the ortho-positions, two Si-atoms at the meta-positions (green) and two Si-atoms at the para-positions [27].

The electronic structure is calculated via the plane-wave projector-augmented wave method implemented in the Quantum Espresso (QE) package [28]. In the QE package, the approach is based on an iterative solution of the Kohn-Sham equation of the DFT theory [29]. In the DFT approach, the generalized gradient approximation (GGA) method, and the exchange-correlation functions are realized in the non-relativistic Perdew-Burke Emzerhof pseudo-potential (PBE) [30]. In addition, The plane-wave basis is arranged to a kinetic energy cut-off equal to 490 eV [31]. The DFT scheme can thus be used to investigate the band structure, the density of state (DOS), and the charge density distribution [32] of the system.

The thermal properties of the system are studied using the Boltzmann theory implemented in the BoltzTraP package [33], where the specific heat, c, of the system can be calculated via

$$c(T;\mu) = \int n(\varepsilon)(\varepsilon - \mu)\left[\frac{\partial f_\mu(T;\varepsilon)}{\partial T}\right] d\varepsilon \tag{1}$$

and the electronic thermal conductivity, κ^0, is determined by

$$\kappa^0_{i,j}(T;\mu) = \frac{1}{e^2 T \Omega} \int \sigma_{i,j}(\varepsilon)(\varepsilon - \mu)^2 \left[-\frac{\partial f_\mu(T;\varepsilon)}{\partial \varepsilon}\right] d\varepsilon \tag{2}$$

where $\sigma_{i,j}(\varepsilon)$ indicates the conductivity tensors, and Ω is the number of
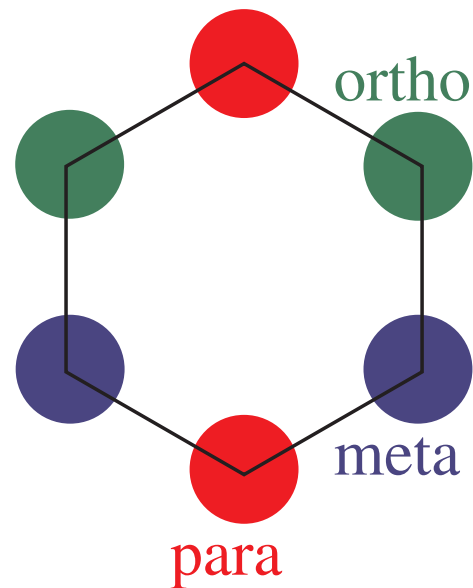

Fig. 1. Schematic diagram indicating the ortho (green), the meta (blue), and the para (red) positions of doping in the honeycomb structure. (For interpretation of the references to colour in this figure legend, the reader is referred to the web version of this article.)

K point which are sampled in Brillouin zone [33].

Results

In this section, we present the main results obtained from the calculations. We start with the pristine graphene nanosheet without an Si-dopant. Initially, we let the system fully relax. After the structural relaxation, the bond length of the C–C atoms is found to be 1.42 Å, and the lattice constant becomes $a = 2.46$ Å, these values are in good agreement with the literature [34]. Fig. 2 displays the pristine graphene nanosheet (left panel) and its charge density distribution (right panel). It seems that the honeycomb structure with the 3×3 supercell is clearly observed in the charge density distribution without any defect or deformation in the crystal structure indicating a pure graphene nanosheet.

The electronic structure of the pristine graphene system is presented in Fig. 3, with the band structure (left panel) and the density of state (right panel). The dashed black line in the energy axis indicates the Fermi level, E_F. As expected, there is no band gap between the valence and the conduction bands at the K point. It turns out that the DOS is zero at the point where the band gap is zero (see Fig. 3 (right panel)). The band structure and the DOS of pristine graphene for different numbers of supercells have been investigated by many research groups, where the zero band gap and the DOS have been predicted for a monolayer [36], a bilayer [37], and a trilayer [18,38]. We note that in our calculations the spin-orbit interaction (SOI) is neglected. In the presence of the SOI, we find a tiny band gap at the K point with a magnitude 0.98 μeV which is in good agreement with an estimate obtained from a tight-binding model [39]. The gap can be referred to the interactions of the π orbital bonds. A bit larger band gap is seen when higher orbits of the carbon atoms are included in the calculations [40].

We now consider Si atoms substitutionally doped in the graphene nanosheet with different geometries or configurations: triangle- and "dot"-shapes. In the triangle Si-doped graphene, we assume three Si atoms (blue color) forming a triangle shape embedded in the center of the graphene nanosheet as is shown in Fig. 4 (top left panel). Two of the Si-atoms are placed at the ortho-positions and the third one is embedded in a para-position forming a triangle shape. In addition, a configuration with six Si-atoms forming a "circle" or a "quantum dot" shape embedded in the center of the graphene nanosheet (bottom left
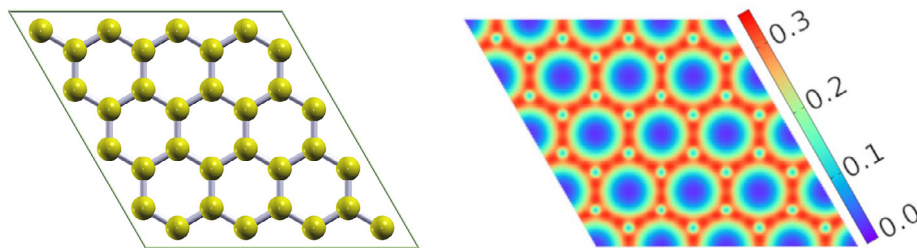
Fig. 2. The pure graphene nanosheet with 3 × 3 supercell (left panel) and the charge density distribution (right panel). The carbon atoms, C, are golden colored. The bond length C–C is 1.42 Å, and the lattice constant is $a = 2.46$ Å. Xcrysden is used to produce the pure graphene supercell (left panel) [35].

panel) is also considered in this study in which the six Si-atoms are distributed over the ortho-, meta-, para-positions.

The configuration and the distribution of embedded Si atoms in graphene have been investigated [41], and it has been shown that the location of Si atoms on the graphene (not the concentration) can easily be used to tune the electronic structure of the system. The Si doped graphene nanosheets are called siligraphene nanosheets [42]. These two selected shapes are analogous to the triangle shape of semiconducting nanowires that have been used to control the efficiency of the solar cells [43] and the quantum dots embedded in semiconductor quantum wires used to design the resulting charge distribution [44–46] and thermoelectric [47] currents. Motivated by these geometrical shapes of the semiconducting materials, we consider the triangle and dot Si-dopant configurations and investigate their electrical and thermal properties.

To check the stability of Si doped graphene we need to calculate the formation energy (E_f) from the below equation

$$E_f = E_T - N_C \mu_C - N_{Si} \mu_{Si}. \tag{3}$$

Herein, E_T is the total energy of the Si doped graphene, N_C and N_{Si} are the number of carbon and silicon atoms in the Si doped graphene, respectively, and μ_C and μ_{Si} are the chemical potentials of the single carbon and single silicon atom, respectively [48,49]. The formation energy of the triangle configuration of Si doped graphene is − 108.701 eV which is smaller than that of the "dot" configuration of the Si doped graphene, − 85.769 eV. The smaller formation energy, the more stable structure is obtained. So, the triangle configuration of the Si doping atoms is more stable than the dot configuration of the Si doping atoms.

We examined the stability of the triangle configuration of the Si dopant structure by moving one Si atom from a para-position to a next neighbor site of a para-position and see that the formation energy becomes − 106.495 eV. It indicates that the stability is slightly reduced by moving away one Si atom from the triangle configuration at the center of the system. In addition, if one Si atom of an ortho-position is moved from the dot configuration to a next neighbor site of an ortho-position, the formation energy is increased to − 75.095 eV. It demonstrates that our model of a dot configuration is more stable. It has been reported that if the positions of doped atoms are varied in a structure with low doping concentration the stability is slightly changed. But for a high doping concentration, changing positions of doping atoms has bigger influences on the stability of the structure [27].

The charge density distribution of the graphene nanosheet with the triangle (top right panel) and the "dot" shape (bottom right panel) are demonstrated in Fig. 4. We should mention that the Si-atoms embedded in the graphene changes the bond length C-C to 1.413 Å in the triangle, and to 1.53 Å in the "dot" structures. The bond length modification of C–C can be referred back to the repulsion force generated between C and Si atoms. These changes influence the charge distribution of the system. It can be clearly seen that in both structures the charge is delocalized around the Si-atoms. This indicates that the Si-atoms loose charge and act as "donors" [50]. The delocalization of charge around the Si-atoms may also be referred to the fact that the Si-atoms have a larger atomic radius than carbon [51]. The delocalization of charge has also been observed in other materials such as semiconductors [52] leading to enhanced transport. The strength of the interaction is thus increased represented by a repulsion force that expels charge away from the center of the siligraphene nanosheet, i.e., charge carriers
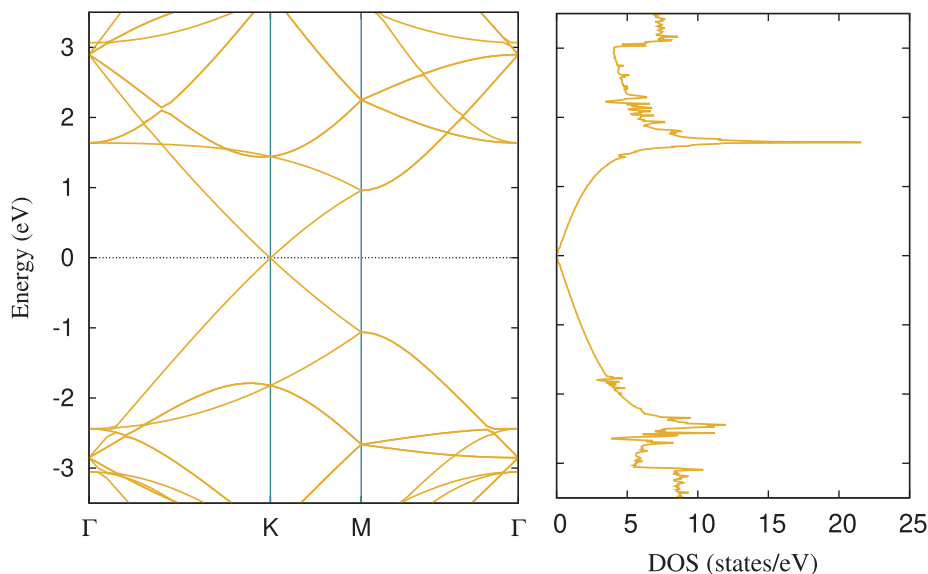

Fig. 3. Band structure (left panel) and the DOS (right panel) of the pristine monolayer graphene nanosheet. The horizontal dashed black line represents the Fermi level, E_F. The bond length C–C is 1.42 Å, and the lattice constant is $a = 2.46$ Å.
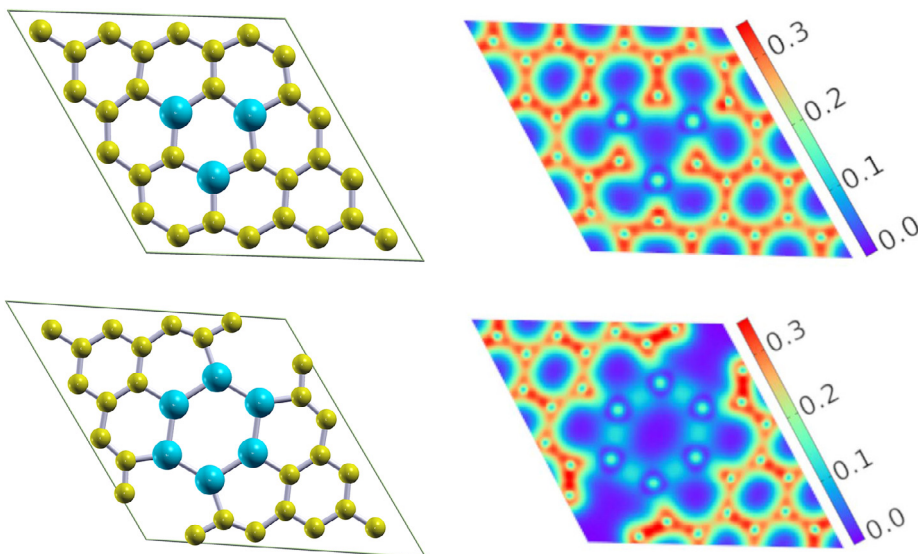
Fig. 4. A graphene nanosheet with a triangle configuration of Si-doping atoms (top left panel) and its charge density distribution (top right panel). Two Si-atoms are located at the ortho-positions while one Si-atom is at the para-position. The graphene nanosheet with the "dot" configuration of Si-doping atoms (bottom left panel) and its charge density distribution (bottom right panel). The six Si-atoms are distributed over the ortho-, meta-, para-positions.

exceed a bit in other places of the system.

Fig. 5 shows the electronic band structure of the triangle (top panel) and the "dot" (bottom panel) Si-doped graphene nanosheet. The repulsion force formed in the presence of triangle Si-dopant opens a band gap, $E_g = 0.448$ eV, at the K point as is seen in Fig. 5 (top panel) [53,54]. This leads to the Si-doped graphene becoming a semiconducting material.

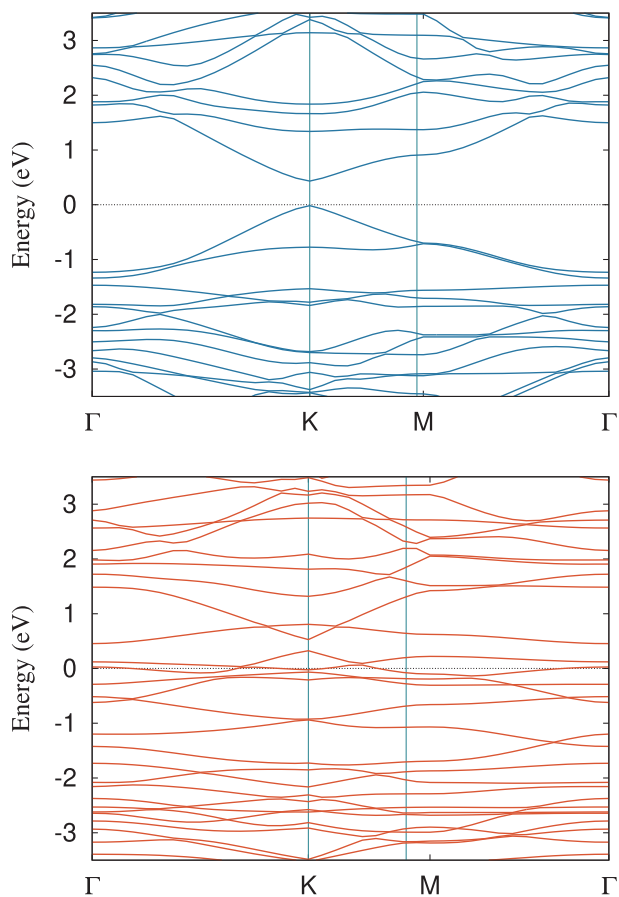The electronic band structure of the "dot" Si-doped graphene gives a totally different physical picture in which valence bands cross the Fermi energy. The crossing energy bands have been predicted for different material structures and it has been demonstrated that the magnitude and the direction of the energy band gap can be sensitively controlled by the dopant type and concentration [55,37]. The crossing band structure is related to the atomic concentration in the primitive unit cell of the Si-doped graphene nanosheet in which the atoms feel almost the same potential energy at a specific ratio of dopant concentration. Consequently, the band gap closes down, and the conduction, or the particulars of the valence band crossing the Fermi level, depend on the dopant type [50,37].

The changes in the band structure will directly influence the DOS as is displayed in Fig. 6 for the graphene with triangle (blue color) and "dot" (red color) Si-dopant. For instance, the DOS vanishes in the range of the band gap for the triangle Si-doped graphene, and the DOS around the Fermi level is increased to finite values for the "dot" Si-doped graphene due to the formation of the Fermi-momentum states.

We now present the thermal properties of the aforementioned structures including the specific heat and the electronic thermal conductivity. The Heat capacity can be calculated or measured by the ratio of the heat added to or removed from the graphene or Si-doped graphene to the resulting temperature change [56]. Therefore, the specific
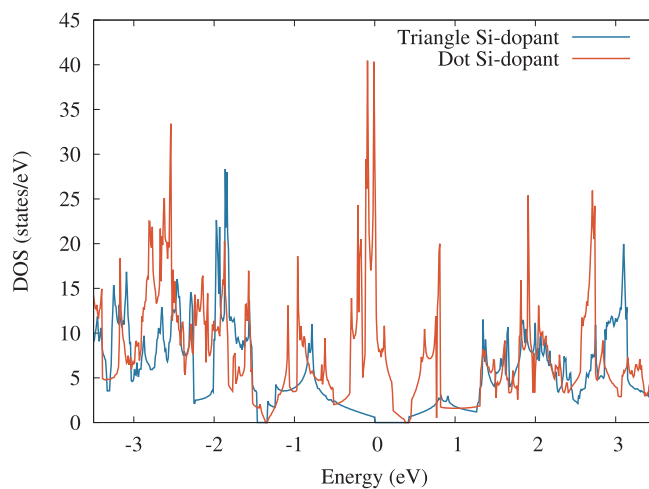

Fig. 5. Calculated electronic band structure of the graphene nanosheet with triangle (top panel) and "dot" shape (bottom panel) Si-dopants. The horizontal dashed black lines represent the Fermi level, E_F.

Fig. 6. Density of state, DOS, of the triangle (blue color) and "dot" (red color) Si-doped graphene nanosheets. (For interpretation of the references to colour in this figure legend, the reader is referred to the web version of this article.)
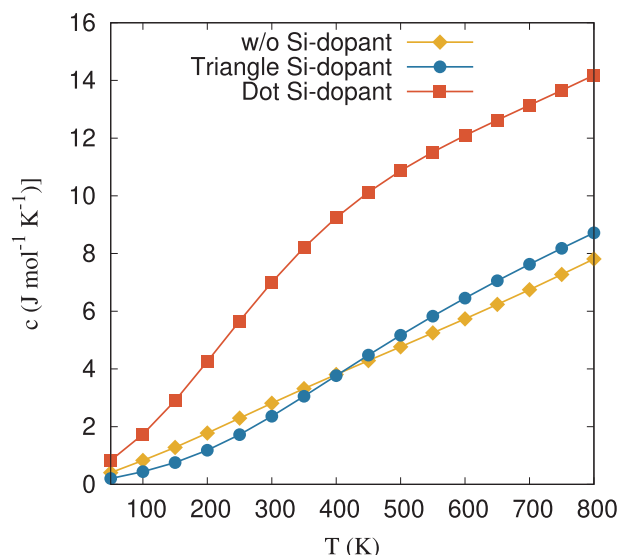
Fig. 7. Specific heat, *c*, for the graphene without (w/o) Si-dopant (golden diamond), and the graphene with triangle (blue circle) and dot (red square) Si-dopant.

Fig. 8. Thermal conductivity, κ^0, for the pristine graphene (golden diamond), and the graphene with triangle (blue circle) and "dot" (red square) Si-dopant. (For interpretation of the references to colour in this figure legend, the reader is referred to the web version of this article.)

heat can be defined as the heat capacity per unit mass of the material. Fig. 7 shows the specific heat, *c*, for the graphene without (w/o) Si-dopant (golden diamond), and the graphene with triangle (blue cir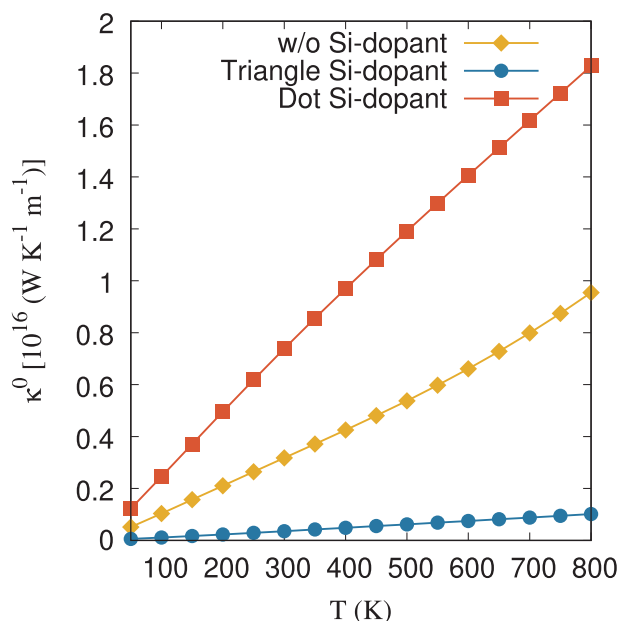cle) and "dot" (red square) Si-dopant. It can be seen that the specific heat increases with the temperature for all three cases. The specific heat for the triangle Si-doped graphene is competing with the pristine graphene structure. Below 400 K the specific heat of the triangle Si-dopant structure is decreased due to the opening band gap that resists the heat transport at "low" temperature. But above 400 K the specific heat is increased compared to the pristine graphene which is related to the effect of high temperature reducing the effective band gap. Furthermore, the specific heat is drastically enhanced for the "dot" Si-doped graphene in which valence bands are crossed by the Fermi energy. The crossing valence bands arise a heat transfer in the system. We should

mention that our calculated specific heat for the pristine graphene is in a good agreement with other calculations of the specific heat for graphene valid for temperatures below 800 K [57].

In Fig. 8 the electronic thermal conductivity is presented for the pristine graphene (golden diamond), and the graphene with triangle (blue circle) and "dot" (red square) Si-doping atoms. The opening of the band gap for the graphene with triangle Si-doping atoms arises less DOS around the Fermi energy. Consequently, the charge carriers is decreased in the selected range of temperatures and the thermal conductivity is thus suppressed compared to the pristine graphene. But the increased DOS in the graphene with dot Si-dopant configuration increases the number of charge carriers and the thermal conductivity is thus enhanced.

Conclusions

We have studied thermal properties of graphene nanosheets with Si atoms with triangle or "dot" shape configuration of dopants. Density functional theory had been used to calculate the band structure, the density of states, and the charge density distribution. We found that the Si-impurities in both doped systems play a donor role giving charge to the graphene structure leading to delocalized charge around the Si-impurities. As a result, a repulsion force in the triangle Si-doped graphene arises a band gap that can be controlled by the concentration of the Si-dopant. The opening band gap in the triangle Si-doped graphene leads to decreases in both the specific heat and the thermal conductivity at low temperatures. Furthermore, as the concentration of silicon atoms is higher in the "dot" Si-doped graphene the induce repulsion forces are higher than in the triangular configuration of dopants. Valence bands thus cross the Fermi-energy in the "dot" Si-doped graphene with resulting increases in the density of state and the number of charge carriers. As a result, the specific heat and the thermal conductivity are enhanced.

Acknowledgment

Appendix A. Supplementary data

Supplementary data associated with this article can be found, in the online version, at https://doi.org/10.1016/j.rinp.2019.102625.

References

[1] Lee C, Wei X, Kysar JW, Hone J. Measurement of the elastic properties and intrinsic strength of monolayer graphene. Science 2008;321(5887):385–8. https://doi.org/10.1126/science.1157996. URL:https://science.sciencemag.org/content/321/5887/385.full.pdf.

[2] Zhang Y, Tan Y-W, Stormer HL, Kim P. Experimental observation of the quantum hall effect and berry's phase in graphene. Nature 2005;438(7065):201–4. https://doi.org/10.1038/nature04235.

[3] Salehi-Khojin A, Estrada D, Lin KY, Ran K, Haasch RT, Zuo J-M, Pop E, Masel RI. Chemical sensors based on randomly stacked graphene flakes. Appl Phys Lett 2012;100(3):033111 .

[4] Avouris P. Graphene: electronic and photonic properties and devices. Nano Lett 2010;10(11):4285–94. pMID: 20879723.

[5] Shahil KMF, Balandin AA. Thermal properties of graphene and multilayer graphene: applications in thermal interface materials. Solid State Commun 2012;152(15):1331–40. URL:http://www.sciencedirect.com/science/article/pii/S0038109812002402.

[6] Novoselov KS, Geim AK, Morozov SV, Jiang D, Zhang Y, Dubonos SV, Grigorieva IV, Firsov AA. Electric field effect in atomically thin carbon films. Science 2004;306(5696):666–9. https://doi.org/10.1126/science.1102896. URL:https://science.sciencemag.org/content/306/5696/666.full.pdf.

[7] Geim AK, Novoselov KS. The rise of graphene. Nat Mater 2007;6:183. https://doi.org/10.1038/nmat1849. EP –.

[8] Allen MJ, Tung VC, Kaner RB. Honeycomb carbon: a review of graphene. Chem Rev 2010;110(1):132–45. pMID: 19610631.

[9] Kroto HW, Heath JR, O'Brien SC, Curl RF, Smalley RE. C60: buckminsterfullerene. Nature 1985;318(6042):162–3. https://doi.org/10.1038/318162a0.

[10] Kroto HW, Buckminsterfullerene C60:. the celestial sphere that fell to earth. Angew Chem Int Ed Engl 1992;31(2):111–29. https://doi.org/10.1002/anie.199201113.

[11] Jalali-Asadabadi S, Ghasemikhah E, Ouahrani T, Nourozi B, Bayat-Bayatani M, Javanbakht S, et al. Electronic structure of crystalline buckyballs: fcc-c60. J Electron Mater 2016;45(1):339–48. https://doi.org/10.1007/s11664-015-4080-2.

[12] Al-Saleh MH. Electrical and mechanical properties of graphene/carbon nanotube hybrid nanocomposites. Synth Met 2015;209:41–6. URL:http://www.sciencedirect.com/science/article/pii/S0379677915300047.

[13] Feng W, Qin M, Lv P, Li J, Feng Y. A three-dimensional nanostructure of graphite intercalated by carbon nanotubes with high cross-plane thermal conductivity and bending strength. Carbon 2014;77:1054–64. URL:http://www.sciencedirect.com/science/article/pii/S0008622314005673.

[14] Enoki T, Fujii S, Takai K. Zigzag and armchair edges in graphene. Carbon 2012;50(9):3141–5. URL:http://www.sciencedirect.com/science/article/pii/S0008622311008232.

[15] Han MY, Brant JC, Kim P. Electron transport in disordered graphene nanoribbons. Phys Rev Lett 2010;104:056801https://doi.org/10.1103/PhysRevLett.104.056801.

[16] Cresti A, Nemec N, Biel B, Niebler G, Triozon F, Cuniberti G, et al. Charge transport in disordered graphene-based low dimensional materials. Nano Res 2008;1(5):361–94. https://doi.org/10.1007/s12274-008-8043-2.

[17] Felix IM, Pereira LFC. Thermal conductivity of graphene-hbn superlattice ribbons. Sci Rep 2018;8(1):2737. https://doi.org/10.1038/s41598-018-20997-8.

[18] Li P, Zhou R, Zeng XC. The search for the most stable structures of silicon-carbon monolayer compounds. Nanoscale 2014;6(20):11685–91. https://doi.org/10.1039/C4NR03247K.

[19] Dong H, Zhou L, Frauenheim T, Hou T, Lee S-T, Li Y. Sic7 siligraphene: a novel donor material with extraordinary sunlight absorption. Nanoscale 2016;8(13):6994–9. https://doi.org/10.1039/C6NR00046K.

[20] Zhou L-J, Zhang Y-F, Wu L-M. Sic2 siligraphene and nanotubes: novel donor materials in excitonic solar cells. Nano Lett 2013;13(11):5431–6. pMID: 24134541.

[21] Pumera M, Sofer Z. Towards stoichiometric analogues of graphene: graphane, fluorographene, graphol, graphene acid and others. Chem Soc Rev 2017;46(15):4450–63. https://doi.org/10.1039/C7CS00215G.

[22] Zhao J, Zhang R. Two-dimensional topological insulators with binary honeycomb lattices: Sic3 siligraphene and its analogs. Phys Rev B 2014;89:195427https://doi.org/10.1103/PhysRevB.89.195427.

[23] Dong H, Wang L, Zhou L, Hou T, Li Y. Theoretical investigations on novel sic5 siligraphene as gas sensor for air pollutants. Carbon 2017;113:114–21. URL:http://www.sciencedirect.com/science/article/pii/S0008622316310028.

[24] Houmad M, Essaoudi I, Ainane A, El Kenz A, Benyoussef A, Ahuja R. Improving the electrical conductivity of siligraphene sic7 by strain. Optik 2019;177:118–22. URL:http://www.sciencedirect.com/science/article/pii/S0030402618312737.

[25] Houmad M, El Kenz A, Benyoussef A. Thermal and electrical properties of siligraphene and its derivatives. Optik 2018;157:936–43. URL:http://www.sciencedirect.com/science/article/pii/S0030402617312056.

[26] Balandin AA. Thermal properties of graphene and nanostructured carbon materials. Nat Mater 2011;10:569. https://doi.org/10.1038/nmat3064. EP –.

[27] Rani P, Jindal VK. Stability and electronic properties of isomers of b/n co-doped graphene. Appl Nanosci 2014;4(8):989–96. https://doi.org/10.1007/s13204-013-0280-3.

[28] Giannozzi P, Baroni S, Bonini N, Calandra M, Car R, Cavazzoni C, et al. J Phys: Condens Matter 2009;21(39):395502 https://doi.org/10.1088/0953-8984/21/39/395502.

[29] Kohn W, Sham LJ. Self-consistent equations including exchange and correlation effects. Phys Rev 1965;140:A1133–8. https://doi.org/10.1103/PhysRev.140.A1133.

[30] Petersen M, Wagner F, Hufnagel L, Scheffler M, Blaha P, Schwarz K. Improving the efficiency of fp-lapw calculations. Comput Phys Commun 2000;126(3):294–309. URL:http://www.sciencedirect.com/science/article/pii/S0010465599004956.

[31] Perdew JP, Burke K, Ernzerhof M. Generalized gradient approximation made simple. Phys Rev Lett 1996;77:3865–8. https://doi.org/10.1103/PhysRevLett.77.3865.

[32] Gudmundsson V, Sitek A, Abdullah NR, Tang C-S, Manolescu A. Cavity-photon contribution to the effective interaction of electrons in parallel quantum dots. Ann Phys 2016;528(5):394–403. https://doi.org/10.1002/andp.201500298.

[33] Madsen GKH, Singh DJ. Boltztrap a code for calculating band-structure dependent quantities. Comput Phys Commun 2006;175(1):67–71. URL:http://www.sciencedirect.com/science/article/pii/S0010465506001305.

[34] Avouris P. Graphene: electronic and photonic properties and devices. Nano Lett 2010;10(11):4285–94. https://doi.org/10.1021/nl102824h.

[35] Kokalj A. Computer graphics and graphical user interfaces as tools in simulations of matter at the atomic scale. Comput Mater Sci 2003;28(2):155–68. https://doi.org/10.1016/S0927-0256(03)00104-6. Proceedings of the Symposium on Software Development for Process and Materials Design.

[36] Chiu YH, Lai YH, Ho JH, Chuu DS, Lin MF. Electronic structure of a two-dimensional graphene monolayer in a spatially modulated magnetic field: Peierls tight-binding model. Phys Rev B 2008;77:045407 https://doi.org/10.1103/PhysRevB.77.045407.

[37] Zollner K, Gmitra M, Fabian J. New J Phys 2018;20(7):073007 https://doi.org/10.1088/1367-2630/aace51.

[38] Uddin S, Chan KS. Band structure of abc-trilayer graphene superlattice. J Appl Phys 2014;116(20):203704. https://doi.org/10.1063/1.4902846.

[39] Yao Y, Ye F, Qi X-L, Zhang S-C, Fang Z. Spin-orbit gap of graphene: first-principles calculations. Phys Rev B 2007;75:041401 https://doi.org/10.1103/PhysRevB.75.041401.

[40] Gmitra M, Konschuh S, Ertler C, Ambrosch-Draxl C, Fabian J. Band-structure topologies of graphene: spin-orbit coupling effects from first principles. Phys Rev B 2009;80:235431 https://doi.org/10.1103/PhysRevB.80.235431.

[41] Wei X-L, Wen X, Xu L-C, Peng X-Y, Liu L-M, Wang R-Z, Cao J-X. Significant interplay effect of silicon dopants on electronic properties in graphene. Phys Lett A 2014;378(26):1841–4. URL:http://www.sciencedirect.com/science/article/pii/S0375960114004277.

[42] Naqvi SR, Hussain T, Luo W, Ahuja R. Metallized siligraphene nanosheets (sic7) as high capacity hydrogen storage materials. Nano Res 2018;11(7):3802–13. https://doi.org/10.1007/s12274-017-1954-z.

[43] Routray S, Shougaijam B, Lenka TR. Exploiting polarization charges for high-performance (000−1) facet gan/ingan/gan core/shell/shell triangular nanowire solar cell. IEEE J Quant Electron 2017;53(5):1–8. https://doi.org/10.1109/JQE.2017.2734078.

[44] Abdullah NR, Tang CS, Manolescu A, Gudmundsson V. Electron transport through a quantum dot assisted by cavity photons. J Phys: Condens Matter 2013;25:465302 .

[45] Abdullah NR, Fatah AH, Fatah JMA. Effects of magnetic field on photon-induced quantum transport in a single dot-cavity system. Chin Phys B 2016;25(11):114206 . URL:http://stacks.iop.org/1674-1056/25/i=11/a=114206.

[46] Abdullah NR, Tang C-S, Manolescu A, Gudmundsson V. Competition of static magnetic and dynamic photon forces in electronic transport through a quantum dot. J Phys: Condens Matter 2016;28(37):375301 . URL:http://stacks.iop.org/0953-8984/28/i=37/a=375301.

[47] Abdullah NR, Marif RB, Rashid HO. Photon-mediated thermoelectric and heat currents through a resonant quantum wire-cavity system. Energies 2019;12(6). https://doi.org/10.3390/en12061082. URL:http://www.mdpi.com/1996-1073/12/6/1082.

[48] Reuter K, Scheffler M. First-principles atomistic thermodynamics for oxidation catalysis: surface phase diagrams and catalytically interesting regions. Phys. Rev. Lett. 2003;90:046103 https://doi.org/10.1103/PhysRevLett.90.046103.

[49] Li P, Zhou R, Zeng XC. The search for the most stable structures of silicon-carbon monolayer compounds. Nanoscale 2014;6:11685–91.

[50] Miao L, Jia R, Wang Y, Kong C-P, Wang J, Eglitis RI, Zhang H-X. Certain doping concentrations caused half-metallic graphene. J Saudi Chem Soc 2017;21(1):111–7. https://doi.org/10.1016/j.jscs.2016.03.007. URL:http://www.sciencedirect.com/science/article/pii/S1319610316300047.

[51] Houmad M, Zaari H, Benyoussef A, El Kenz A, Ez-Zahraouy H. Optical conductivity enhancement and band gap opening with silicon doped graphene. Carbon 2015;94:1021–7. URL:http://www.sciencedirect.com/science/article/pii/S0008622315300567.

[52] Abdullah NR, Tang CS, Manolescu A, Gudmundsson V. Delocalization of electrons by cavity photons in transport through a quantum dot molecule. Physica E 2014;64:254–62.

[53] Sahu S, Rout GC. Band gap opening in graphene: a short theoretical study. Int Nano Lett 2017;7(2):81–9. https://doi.org/10.1007/s40089-017-0203-5.

[54] Shi Z, Zhang Z, Kutana A, Yakobson BI. Predicting two-dimensional silicon carbide monolayers. ACS Nano 2015;9(10):9802–9. https://doi.org/10.1021/acsnano.5b02753.

[55] Tsai S-J, Yang R-J. Bimodal behaviour of charge carriers in graphene induced by electric double layer. Scientific Rep 2016;6:30731. https://doi.org/10.1038/srep30731. EP –.

[56] Wang J, Xie H, Guo Z, Guan L, Li Y. Improved thermal properties of paraffin wax by the addition of tio2 nanoparticles. Appl Therm Eng 2014;73(2):1541–7. URL:http://www.sciencedirect.com/science/article/pii/S1359431114004542.

[57] Wang J, Xie H, Guo Z. First-principles investigation on thermal properties and infrared spectra of imperfect graphene. Appl Therm Eng 2017;116:456–62. URL:http://www.sciencedirect.com/science/article/pii/S135943111632542X.